

On strong correlation between shifted velocity and line width of broad blue-shifted [O III] components in quasars

XUEGUANG ZHANG¹

¹*School of Physics and technology, Nanjing Normal University, No. 1, Wenyuan Road, Nanjing, 210023, P. R. China*

Submitted to ApJ

ABSTRACT

In this manuscript, we report strong linear correlation between shifted velocity and line width of the broad blue-shifted [O III] components in SDSS quasars. Broad blue-shifted [O III] components are commonly treated as indicators of outflows related to central engine, however, it is still an open question whether the outflows are related to central accretion properties or related to local physical properties of NLRs (narrow emission line regions). Here, the reported strong linear correlation with the Spearman Rank correlation coefficient 0.75 can be expected under the assumption of AGN (active galactic nuclei) feedback driven outflows, through a large sample of 535 SDSS quasars with reliable blue-shifted broad [O III] components. Moreover, there are much different detection rates for broad blue-shifted and broad red-shifted [O III] components in quasars, and no positive correlation can be found between shifted velocity and line width of the broad red-shifted [O III] components, which provide further and strong evidence to reject possibility of local outflows in NLRs leading to the broad blue-shifted [O III] components in quasars. Thus, the strong linear correlation can be treated as strong evidence for the broad blue-shifted [O III] components as better indicators of outflows related to central engine in AGN. Furthermore, rather than central BH masses, Eddington ratios and continuum luminosities have key roles on properties of the broad blue-shifted [O III] components in quasars.

Keywords: galaxies:active - galaxies:nuclei - quasars:emission lines

1. INTRODUCTION

Active Galactic Nuclei (AGN) driven outflows, as the probe of AGN feedback, have been studied in detail for more than two decades (Crenshaw et al. 2003; Veilleux et al. 2005; Fabian 2012; Page et al. 2012; King & Pounds 2015; Cheung et al. 2016; Martin-Navarro et al. 2018). AGN feedback driven outflows not only show clear linkages between AGN and host galaxies, such as AGN feedback model expected M-sigma relations (Ferrarese & Merritt 2000; Gebhardt et al. 2000; Kormendy & Ho 2013) indicating mass outflowing leading to the strong physical connections between central black hole (BH) masses and host galaxy properties, but also strongly indicate outflows from central regions have apparent and important effects on structures of emission/absorption lines from both NLRs (narrow emission line regions) and BLRs (broad emission line regions).

Blue-shifted [O III] emission features have been widely treated as indicators of outflows on scale of kpcs around NLRs in AGN, besides broad absorption lines in UV and

X-ray bands as better indicators of outflows coming from central accretion disk winds in AGN on scale of light-months to light-years (around central BLRs) (Ganguly et al. 2007; Tombesi et al. 2015). Sergeev et al. (1997) have shown that broad wings of [O III] emission lines could be emitted from the outer BLRs and suggested the presence of an outflow component, through study of variations of the [O III] line profiles in NGC5548. Tadhunter et al. (2001) have shown that kinematics of the broad blue-shifted [O III] emission lines are consistent with outflow in an inner NLRs in PKS1549-79. Gupta et al. (2005) have shown that kinematic properties of the blue-shifted absorption-line system (relative to the emission-line system) are similar to the blue-shifted [O III] lines, indicating strong connections with outflowing materials in 3C48. Holt et al. (2008) have discussed fast outflows in compact radio sources, through properties of broad blue-shifted [O III] components. Mullaney et al. (2013) have shown that the [O III] profiles of type-1 and type-2 AGN show the same trends in terms of line width, but type-1 AGN display a much stronger blue wings, which can be well interpret as evidence of outflowing ionized gases. Perna et al. (2015) have detected galaxy-wide outflows in high redshift lu-

minous obscured quasars by properties of broad [O III] lines. [Zakamska et al. \(2016\)](#) have shown that broad [O III] emission regions on a few kpc scales can be affected by extreme outflow from central regions through a sample of high redshift red quasars. However, not similar as broad absorption lines tightly related to outflows from central disk winds, local physical properties in NLRs can also lead to blue-shifted features in [O III] emission lines, such as local flows in NLRs related to stellar winds. Certainly, there are some reported results indicating blue-shifted [O III] components could be possibly related to central engine. [Boroson \(2005\)](#) have shown weak dependence of shifted velocities of blue-shifted [O III] components on line width of [O III] lines through a sample of about 800 quasars in SDSS DR1 (Sloan Digital Sky Survey, Data Release 1) ([Abazajian et al. 2003](#)). [Schmidt et al. \(2018\)](#) have shown much loose correlation between shifted velocities of blue-shifted [O III] components and line widths of [O III] lines through a sample of 28 narrow line Seyfert I galaxies, much similar weak trends can also be found in [Woo et al. \(2016\)](#); [Eun et al. \(2017\)](#) in samples of type 2 AGN and hidden type-1 AGN.

More and more evidence have shown that broad blue-shifted [O III] components rather than the core [O III] components are more tightly related to central engine in AGN, such as our previous results in [Zhang et al. \(2017\)](#) and previous results in [Zakamska et al. \(2016\)](#), strongly indicating that broad [O III] emission regions are very nearer to central regions and have stronger luminosity dependence on central continuum emissions in AGN. In the manuscript, unless otherwise stated, the broad [O III] components mean the emissions from the non-BLR regions. Thus, it is interesting to check whether are there apparently stronger evidence to support the broad blue-shifted [O III] emission components, rather than the blue-shifted asymmetric properties determined from the full [O III] as discussed in the literature, treated as indicators of outflows from central regions in AGN. Certainly, after considering probably serious obscuration on broad [O III] emissions in type-2 AGN, we will do our study through a sample of broad line AGN. And the manuscript is organized as follows. In section 2, we show our sample selection and emission line fitting procedure. In Section 3, we show our main results on properties of broad [O III] components in a large sample of SDSS quasars in DR12 (Data Release 12, [Alam et al. \(2015\)](#)). In section 4, the main discussions are given. Then, in Section 5, we show our main conclusions. And in this manuscript, we have adopted the cosmological parameters of $H_0 = 70 \text{ km} \cdot \text{s}^{-1} \text{ Mpc}^{-1}$, $\Omega_\Lambda = 0.7$ and $\Omega_m = 0.3$.

2. SAMPLE SELECTION AND EMISSION LINE FITTING PROCEDURE

The work is based on a large sample of quasars with broad shifted [O III] emission components relative to narrow core

[O III] components. So that, there are three steps to create our main sample. The first step is to create a parent sample of quasars. The second step is to measure necessary line parameters, especially parameters of [O III] emission lines. And the third step is to create our final main sample including objects with reliable broad blue-shifted [O III] emission components, based on reliable measured parameters.

SDSS SkyServer provided SQL (Structured Query Language) Search tool (<http://skyserver.sdss.org/dr12/en/tools/search/sql.aspx>) is firstly applied to conveniently collect SDSS quasars ([Richards et al. 2002](#); [Ross et al. 2012](#)) from SDSS DR12 to create the parent sample. The applied query is as follows:

```
SELECT plate , fiberid , mjd
FROM SpecObjall
WHERE class = 'QSO' and z < 0.65 and
      zwarning = 0 and snmedian > 20
```

, where "SpecObjall" represents the SDSS provided dataset including basic information (redshift, classification, signal-to-noise (SN) of spectra, etc.) of all objects in SDSS DR12. The query leads to collection of 3735 SDSS quasars with reliable redshift less than 0.65 and with high quality spectra with median SN larger than 20. The criterion of $z < 0.65$ is applied to ensure [O III] emission lines totally covered in SDSS spectra. The criterion of median $SN > 20$ on the full observed spectrum can lead to more neat and clean spectroscopic emission line features.

The second step is to measure necessary emission line parameters for the quasars in the parent sample. Similar as what we have done in [Zhang \(2014\)](#); [Zhang et al. \(2016\)](#); [Rakshit et al. \(2017\)](#); [Zhang et al. \(2019\)](#), the most commonly accepted SSP method ([Bruzual & Charlot 2003](#); [Kauffmann et al. 2003](#); [Cid Fernandes et al. 2005](#)) has been firstly applied to a small number of the collected SDSS quasars (especially the low redshift quasars with $z < 0.35$) of which spectra probably include apparent contributions of stellar lights, by considering broadened stellar templates plus a power law component. The 39 simple stellar population templates from [Bruzual & Charlot \(2003\)](#) have been exploited with the population ages from 5 Myr to 12 Gyr and with three solar metallicities ($Z = 0.008, 0.05, 0.02$), which can be used to well-describe the characteristics of almost all the SDSS galaxies as detailed discussions in [Bruzual & Charlot \(2003\)](#). Through the Levenberg-Marquardt least-squares minimization technique (the MPFIT procedure) applied to the SDSS spectra with the emission lines being masked out, the stellar velocity dispersions can be determined by the broadened velocities to the stellar templates, and then the stellar component and the AGN power law continuum component can be clearly determined and separated. Here, we have not only masked out all the listed 24 narrow emissions lines with rest central wavelengths larger than 3700 \AA in <http://classic.sdss.org/dr1/algorithms/speclinefits.html#linelist>

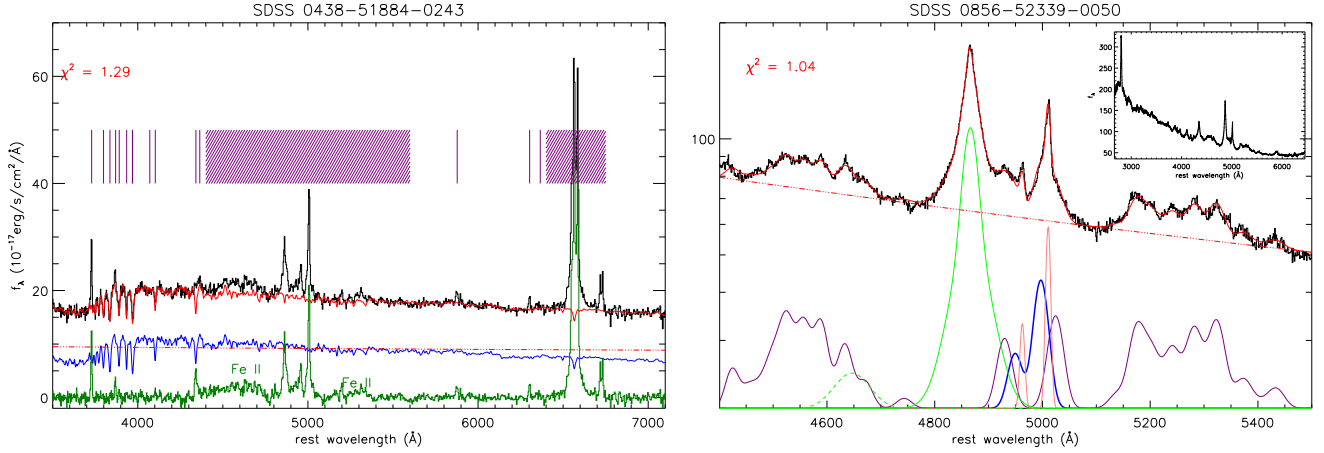


Figure 1. Left panel shows the SSP method determined stellar lights in the quasar SDSS 0438-51884-0243. Right panel shows the best fitted results to the emission lines around $H\beta$ in the quasar SDSS 0856-52339-0050. In left panel, from top to bottom, solid lines in black and in red show the observed SDSS spectrum and the best fitted results by broadened stellar templates plus a power law component, double-dot-dashed red line shows the determined power law AGN continuum emissions, solid blue line shows the determined stellar lights, solid green line shows the pure line spectrum after subtractions of both stellar lights and the AGN continuum emissions. When the SSP method is applied, the emission lines masked out are marked by the vertical lines in purple and in the two areas filled by purple lines. From left to right, the vertical lines in purple mark the following emission features masked out, including [O II] $\lambda 3727\text{\AA}$, $H\theta$, $H\eta$, [Ne III] $\lambda 3869\text{\AA}$, He I $\lambda 3891\text{\AA}$, Calcium K line, [Ne III] $\lambda 3968\text{\AA}$, Calcium H line, [S II] $\lambda 4070\text{\AA}$, $H\delta$, $H\gamma$, [O III] $\lambda 4364\text{\AA}$, He I $\lambda 5877\text{\AA}$ and [O I] $\lambda 6300, 6363\text{\AA}$, respectively. The area filled by purple lines around 5000\AA shows the region masked out including the emission features of optical Fe II lines, broad and narrow $H\beta$ and [O III] doublet, and the area filled by purple lines around 6550\AA shows the region masked out including the emission features of broad and narrow $H\alpha$, [N II] and [S II] $\lambda 6717, 6731\text{\AA}$ doublets. The determined χ^2 value of 1.29 for the best fitted results is marked in the top-left corner in left panel. In the right panel, from top to bottom, solid black line shows the observed line spectrum, solid red line shows the determined best fitted results, double-dot-dashed red line shows the determined power law continuum emissions, solid green line shows the determined broad $H\beta$, solid purple line shows the determined optical Fe II lines, dashed green line shows the determined broad He II line, solid pink line shows the determined core [O III] components, and thick blue solid line shows the determined broad blue-shifted [O III] components. The top-right corner shows the observed blue spectrum of SDSS 0856-52339-0050, in order to clearly show there are few contributions of stellar lights in the spectrum. And the calculated χ^2 value of 1.04 for the best fitted results is marked in the top-left corner in the right panel.

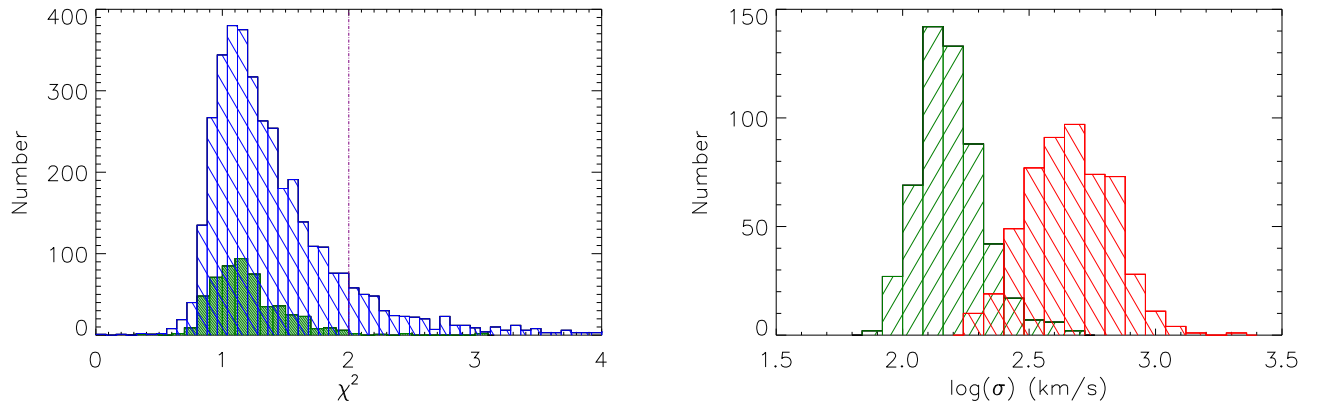


Figure 2. Left panel shows the distribution of χ^2 for the best fitted results to the emission lines in all the collected 3735 quasars (histogram in blue) and in the 535 quasars with reliable broad [O III] components (histogram in dark green). Vertical red line shows the position of $\chi^2 = 2$. Right panel shows the distributions of line width of the broad (histogram in red) and the core (histogram in dark green) [O III] components of the 535 quasars.

with widths of about 450km/s, mainly including the [O II] λ 3727Å, narrow H α , narrow H β , narrow H γ , narrow H δ , [O III] λ 4364Å, [O III] λ 4959, 5007Å, [O I] λ 6300, 6363Å, [N II] λ 6548, 6583Å and [S II] λ 6716, 6731Å, etc., but also masked out the optical Fe II lines and the broad H α and H β . Based on the model determined stellar velocity dispersions and uncertainties (the returned best-fit parameters and the returned PERROR in the MPFIT procedure), the criterion that stellar velocity dispersions larger than 70km/s and smaller than 350km/s at least 5 times larger than their corresponding uncertainties have been applied to determine that the determined stellar components are reliable enough. Here, we do not show further discussions on the SSP method, but the left panel of Fig. 1 shows an example on the SSP method determined stellar lights in the SDSS quasar PLATE-MJD-FIBERID=0438-51884-0243.

After necessary subtractions of contributions of stellar lights, emission lines in line spectrum can be well described. Here, we mainly consider emission lines around H β with rest wavelength range from 4400Å to 5600Å, including broad H β , narrow H β , core and broad [O III] components, broad He II and broad optical Fe II lines. The emission features are fitted simultaneously by the following model functions. There are two (or more if necessary, after checking fitted results) broad Gaussian functions $G_{B1} + G_{B2}$ applied to describe broad H β . Here, each Gaussian function includes three parameters of central wavelength, second moment (width of the component) and line flux. And we accepted the central wavelengths of the two broad H β components in the range of 4800Å to 4900Å. There are three narrow Gaussian functions $G_{NH} + G_{CO31} + G_{CO32}$ applied to describe the narrow H β and core [O III] components, with the central wavelength of narrow H β in the range of 4840Å to 4880Å, and with the flux ratio of core [O III] component tied to the theoretical value of 3 (Dimitrijevic et al. 2007), and with the central wavelengths of the three narrow components tied to be 4862.81Å:4960.295Å:5008.24Å, and with the core [O III] components to have the same line width. There are two another Gaussian functions $G_{BO31} + G_{BO32}$ applied to describe the broad [O III] components, with the central wavelength of the broad [O III] λ 5007Å in the range of 4980Å to 5030Å, and with the broad [O III] components to have the same redshift, the same line width, and to have the flux ratio tied to the theoretical value of 3. There is one broad Gaussian function G_{HeII} applied to describe weak He II line, with the central wavelength in the range of 4600Å to 4730Å. There is one power law function $P_\lambda = \alpha \times (\lambda/5100\text{Å})^\beta$ applied to describe AGN continuum emissions. The broadened and scaled Fe II templates discussed in Kovacevic et al. (2010) Fe_{temps} is applied to describe probable optical Fe II lines. Finally, the

detailed model functions are

$$Y_{\text{model}} = G_{B1} + G_{B2} + G_{NH} + G_{CO31} + G_{CO32} + G_{BO31} + G_{BO32} + G_{HeII} + P_\lambda + Fe_{\text{temps}} \quad (1)$$

. Based on the widely applied Levenberg-Marquardt least-squares minimization technique, the best fitted results to the emission lines can be well determined, and the line parameters and corresponding uncertainties can also be well determined. Here, the uncertainties are the formal 1σ errors computed from the covariance matrix for the final determined best-fit model parameters returned by MPFIT procedure (<http://cow.physics.wisc.edu/~craigm/idl/idl.html>). Then, for the objects with the calculated $\chi^2 = SSR/Dof > \sim 2$ (where SSR and Dof as summed squared residuals and degree of freedom, respectively)¹, the best fitted results have been carefully re-checked by eyes, in order to determine whether the fitting procedure should be re-applied with more than two broad components to describe the broad H β . Right panel of Fig. 1 shows one example on the best fitted results to the emission lines in the quasar SDSS 0856-52339-0050. And the distribution of final determined χ^2 has been shown in the left panel of Fig. 2 for all the 3735 quasars.

Furthermore, in order to find more robust uncertainties of the line parameters, the commonly applied Maximum Likelihood Method (MEM) through the MCMC (Markov Chain Monte Carlo) technique (Foreman-Mackey et al. 2013) has been accepted to re-fit the emission lines with the starting values of model parameters to be the values determined by the MPFIT procedure. Then, the MCMC technique determined posterior distribution can provide optional uncertainty of each model parameter. Here, as an two examples, Fig. 3 shows the MEM determined best fitted results (which are totally similar as the MPFIT procedure determined best fitted results) to the emission lines around H β in SDSS 0856-52339-0050 and in SDSS 1782-53299-0170. For the broad [O III] component in SDSS 0856-52339-0050, the central rest wavelength and the line width can be determined as $4997.09 \pm 0.40\text{Å}$ and $781 \pm 25\text{km/s}$ based on the MCMC technique determined posterior distributions. Meanwhile, the MPFIT procedure determined rest central wavelength and line width of the broad [O III] component are $4997.06 \pm 0.84\text{Å}$ and $789 \pm 27\text{km/s}$. There are similar uncertainties in the line width by the MCMC technique and by the MPFIT procedure, but smaller uncertainties in the rest central wavelength by the MCMC technique. However, for the broad [O III] component in SDSS 1782-53299-0170, the determined rest central wavelength and line width of the broad [O III] component are $(5007.73 \pm 0.05\text{Å}$ and $5007.85 \pm 0.23\text{Å})$ and $(536 \pm 4\text{km/s}$ and $535 \pm 15\text{km/s})$ through the MPFIT procedure and through the

¹ Among the collected 3735 SDSS quasars, there are 447 quasars with the best fitted results leading to χ^2 larger than 2.

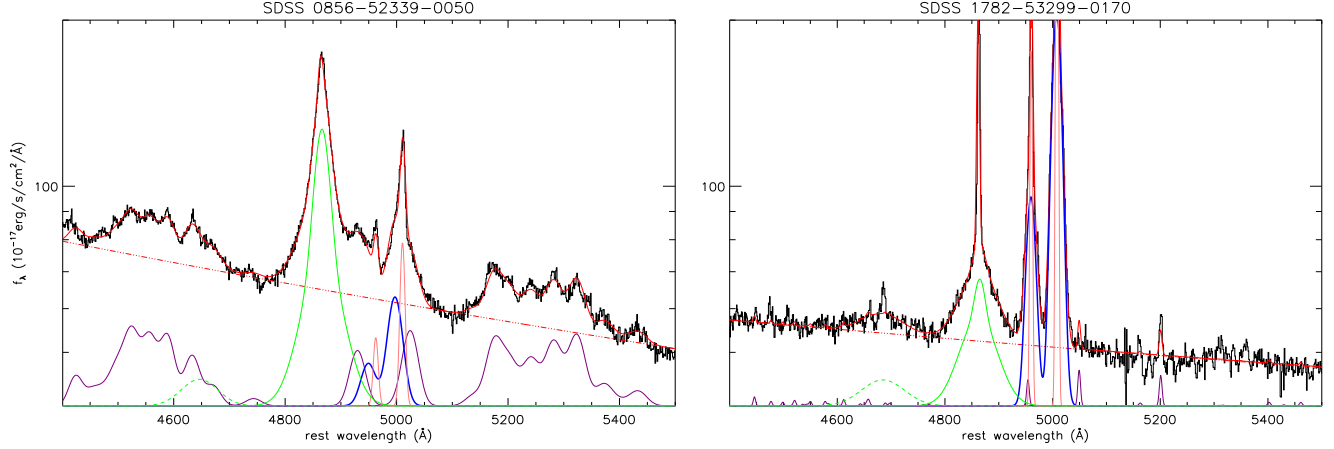


Figure 3. Two examples on the MEM determined best fitted results to the emission lines around H β in SDSS 0856-52339-0050 (left panel) and in SDSS 1782-53299-0170 (right panel). In each panel, line styles have the same meanings as those shown in the right panel of Fig. 1, but the solid red line shows the MEM determined best fitted results.

MCMC technique, respectively, the uncertainties through the MCMC technique are about 4 times larger than the uncertainties determined by the MPFIT procedure. Therefore, different techniques can lead to different uncertainties of the model parameters. And in the manuscript, between the uncertainties determined by the MCMC technique and by the MPFIT procedure for each model parameter, the larger uncertainty has been accepted as its final uncertainty.

Based on the measured line parameters and corresponding uncertainties of the core and the broad [O III] components, the broader component is accepted as the broad [O III] component, and the narrower component is accepted as the core [O III] component, and the shifted velocities of broad [O III] components relative to the core [O III] components can be calculated by $\Delta V = \lambda_{0, \text{core}} - \lambda_{0, \text{broad}}$, with the uncertainties of ΔV determined by $\delta(\Delta V) = \delta(\lambda_{0, \text{core}}) + \delta(\lambda_{0, \text{broad}})$, where $\lambda_{0, \text{core}}$ and $\lambda_{0, \text{broad}}$ mean the measured central wavelengths of the core and the broad [O III] components, and $\delta(\lambda_{0, \text{core}})$ and $\delta(\lambda_{0, \text{broad}})$ are the corresponding uncertainties of the central wavelengths. Then, the following three criteria are applied to collect quasars with reliable broad blue-shifted [O III] components. First, the measured parameters of broad H β are at least 5 times larger than their corresponding uncertainties. Second, the measured line parameters of both core and broad [O III] components are at least 5 times larger than their corresponding uncertainties. Third, the shifted velocities ΔV are at least 5 times larger than their corresponding uncertainties: $\Delta V > 5 \times \delta(\Delta V)$. Based on the three criteria, in our final main sample, there are 535 quasars with reliable broad blue-shifted [O III] components. Best fitted results to the emis-

sion lines in all the 535 quasars can be downloaded² from <https://pan.baidu.com/s/1gG85QpuXBDfa4NRb5dQH9g>.

The measured line parameters of the 535 quasars have been listed in Table 1. And the distribution of final determined χ^2 for the best fitted results to the emission lines has been also shown in the left panel of Fig. 2 for the 535 quasars.

Meanwhile, right panel of Fig. 2 shows distributions of the measured line widths of the broad and core [O III] components of the collected 535 quasars. In the manuscript, we have accepted second moments as the line widths of the core and broad [O III] components. And the maximum line width is about 507 km/s of the core [O III] components, but the maximum line width is about 1981 km/s of the broad [O III] components. Fig. 4 shows distributions of redshift and continuum luminosity at 5100 Å ($L_{\text{con}} = \lambda L_{5100\text{Å}}$) of the 535 quasars. The continuum luminosity L_{con} is calculated based on the continuum flux at rest wavelength of 5100 Å through the determined power law function to describe the AGN continuum emissions underneath broad H β (such as the component shown as double-dot-dashed red line in the right panel of Fig. 1), after subtractions of necessary stellar lights. The

²The access code is xip3. There are three files included in the compressed file "Blue_O3.tar.gz". One file "par_all_tex.list" includes the necessary parameters of the 535 quasars. One PDF file "all_spec.pdf" (13M) shows the results on the determined stellar lights in the spectra of the 535 SDSS quasars with reliable broad blue-shifted [O III] components. Among the 535 SDSS quasars, there are 26 SDSS quasars of which spectra include apparent contributions of stellar lights. In the 26 panels with reliable stellar lights, line styles have the same meanings as those shown in the left panel of Figure 1. In the other panels, only the full SDSS spectra are shown. One PDF file "all_line.pdf" (21M) shows the results on the corresponding best fitted results to the emission lines around H β in the line spectra. And the line spectra of the 26 quasars are determined by subtractions of the stellar lights from the observed SDSS spectra. There are 17 pages in each PDF file, 32 panels per page.

mean redshift and continuum luminosity are about 0.323 and 3.02×10^{44} erg/s, respectively.

Before proceeding further, there is one point we should note. In some quasars, the broad [O III] components have line width σ around 1000 km/s, such as the line width about $\sigma \sim 800$ km/s of the broad blue-shifted [O III] components in the SDSS 0856-52339-0050 shown in the right panel of Fig. 1, which are very large values for narrow emission lines, leading to the question whether should the determined broad [O III] components be actually as part of broad H β from normal BLRs? We rejected the possibility by the following consideration. We have checked the low-redshift quasars with $z < 0.35$ and with reliable broad [O III] components. If the broad [O III] components were part of broad H β , then similar and corresponding stronger features could be found in the red wings of broad H α . However, none low redshift quasars have shown such strong features in the red wings of broad H α . Thus, in the manuscript, we safely accepted that the determined broad [O III] components are truly from [O III] emission regions.

3. MAIN RESULTS

Based on the well measured line parameters, properties of the broad blue-shifted [O III] components can be well checked in the 535 quasars. Fig. 5 shows the correlation between blue-shifted velocity ΔV and line width σ of the broad blue-shifted [O III] components. A strong linear correlation can be confirmed with Spearman Rank correlation coefficient of 0.75 with $P_{null} < 10^{-20}$. Under considering uncertainties in both coordinates, through the Least Trimmed Squares (LTS) robust technique discussed in Cappellari et al. (2013), the correlation can be well described by

$$\log\left(\frac{\sigma}{\text{km/s}}\right) = (1.29 \pm 0.07) + (0.54 \pm 0.03) \times \log\left(\frac{\Delta V}{\text{km/s}}\right) \quad (2)$$

, with rms scatter of about 0.096 in the space of $\log(\sigma)$ versus $\log(\Delta V)$. In order to ensure the strong linear correlation without effects of quality of measured parameters, among the 535 quasars, the 160 quasars with parameters (line width and shift velocity) at least 10 times larger than their corresponding uncertainties are applied to show the correlation again in Fig 5 as red dots. The strong linear correlation can be re-confirmed with Spearman Rank correlation coefficient of 0.64 with $P_{null} \sim 10^{-20}$ for the 160 high-quality quasars, with the corresponding rms scatter of about 0.082.

It is very interesting that it is so-far the first report on so strong linear correlation between ΔV and σ in broad blue-shifted [O III] components. The strong linear correlation not similar as the weak trends in previous references (such as the result in Eun et al. (2017); Schmidt et al. (2018)) are mainly due to the following two points. On the one hand, the line parameters are measured from the well determined Gaussian

broad [O III] components, not similar as the asymmetric parameters previously determined from the full [O III] lines. On the other hand, quasars rather than type-2 AGN (or hidden type-1 AGN) are considered, leading to much wide parameter range of the shifted velocities of broad blue-shifted [O III] components. Based on the strong linear correlation shown in Fig 5, the following points have been considered.

First and foremost, whether the strong linear correlation can be treated as strong evidence for outflows related to central engine but not from local flows in NLRs? Actually, local flows in NLRs could lead to similar detection rates for broad blue-shifted [O III] components and for broad red-shifted [O III] components in quasars. However, based on the similar criteria to collect quasars with reliable broad blue-shifted broad [O III] components, the criteria are applied to collect quasars with reliable broad red-shifted [O III] components: $P_{H\beta} > 5 \times \delta(P_{H\beta})$, $P_{core} > 5 \times \delta(P_{core})$, $P_{broad} > 5 \times \delta(P_{broad})$ and $\Delta V = \lambda_{0, broad} - \lambda_{0, core} > 5 \times (\delta(\lambda_{0, core}) + \delta(\lambda_{0, broad}))$ where P and $\delta(P)$ represent the measured parameters and the corresponding uncertainties, the suffixes of "H β ", "core" and "broad" mean the parameters and the uncertainties for the broad H β , the core [O III] and the broad [O III] components, then there are only 20 quasars with reliable broad red-shifted [O III] components. The much different detection rates strongly and naturally indicate that the broad blue-shifted [O III] components are due to outflows related to central engine rather than due to local flows in NLRs in quasars. Furthermore, for the broad red-shifted [O III] components, the correlation between ΔV and σ is very weak with correlation coefficient of about -0.28. Besides the much different detection rates, the much different correlations between ΔV and σ for the broad blue-shifted and the broad red-shifted [O III] components can also strongly indicate the broad blue-shifted [O III] components are due to outflows related to central engine rather than due to local flows in NLRs.

Besides, whether the large shifted velocities of broad blue-shifted [O III] components can be expected by outflows related to central engine? As the shown results in Fig. 5, the mean shifted velocity of the broad blue-shifted [O III] components of the 535 quasars is about 374 km/s with minimum value about 56 km/s and maximum value about 1440 km/s. The strong dependence of radial velocities of outflowing clouds on distance to central region clearly show that radial velocities on scale of kpcs are about several hundreds of kilometers per second (see the discussed results in King et al. (2011); King & Pounds (2015); Tombesi et al. (2015)), similar as the values shown in Fig. 5. Thus, the large shifted velocities are reasonable under the assumption of AGN-feedback driven outflows.

Last but not the least, whether AGN-feedback driven outflows can be applied to explain the strong correlation shown in Fig 5 for the broad blue-shifted [O III] components in

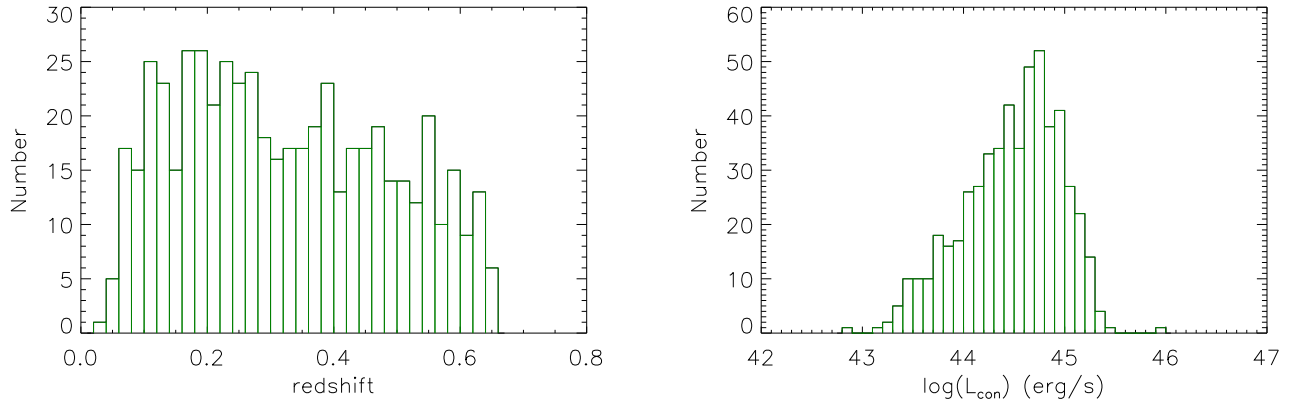


Figure 4. Distributions of redshift (left panel) and continuum luminosity at 5100Å (right panel) of the 535 quasars in our final sample.

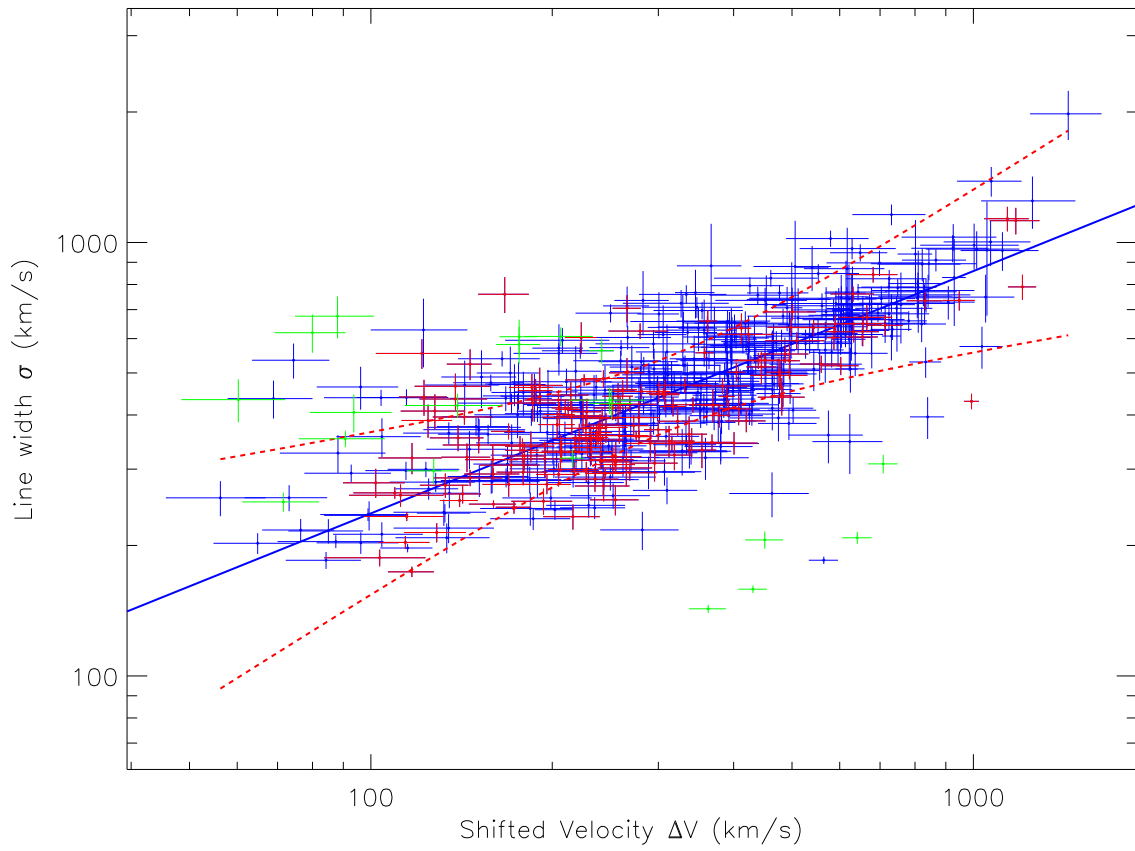


Figure 5. On the correlation between ΔV and line width σ of the broad [O III] components in the quasars. Blue dots plus error bars show the results for all the 535 quasars, red dots plus error bars show the results for the 160 high-quality quasars. Solid blue line and dashed red lines represent the best fitted results for all the 535 quasars, and the corresponding 5σ confidence bands, respectively. Green dots plus error bars represent the results for reliable broad red-shifted [O III] components in the 20 quasars.

quasars? Under the framework of AGN-feedback driven outflows, on scale of kpcs, radial velocities do strongly depend on distance R to central regions, $\Delta V \propto R^{-\alpha}$ with $\alpha > 0$ (such as the results in King et al. (2011)). Moreover, if we accepted that the line width of the broad blue-shifted [O III] components were due to gravitational potential of central BH because of the emission regions nearer to central BH, we could have $\sigma^2 \propto R^{-1}$. Therefore, we can expect the strong correlation between ΔV and σ shown in Fig. 5: $\sigma \propto (\Delta V)^{0.5}$, if $\alpha \sim 1$ accepted. Unfortunately, we can not find an exact mathematical solution to the results shown in Fig. 5 based on the AGN-feedback driven outflow model, due to much complicated initial physical conditions.

4. DISCUSSIONS

In the section, some further discussions have been shown on the dependence of the strong linear correlation shown in Fig. 5 on the other physical parameters, such as Eddington ratio, BH mass, etc.. The virial BH mass M_{BH} can be well determined by the line parameters of broad H β (Greene & Ho 2005; Vestergaard & Peterson 2006; Shen et al. 2011) under the Virialization assumption to broad line emission clouds (Peterson et al. 2004),

$$\frac{M_{\text{BH}}}{M_{\odot}} = 3.6 \times 10^6 \times \left(\frac{L_{\text{H}\beta}}{10^{42} \text{erg/s}} \right)^{0.56} \times \left(\frac{FWHM_{\text{H}\beta}}{1000 \text{km/s}} \right)^2 \quad (3)$$

, where $L_{\text{H}\beta}$ and $FWHM_{\text{H}\beta}$ represent the line luminosity and full width at half maximum of broad H β , respectively. The Eddington ratio \dot{M}_{Edd} can be applied to trace intrinsic accretion rate and estimated by

$$\dot{M}_{\text{Edd}} = \frac{10 \times L_{5100}}{1.4 \times 10^{38} M_{\text{BH}}/M_{\odot}} \quad (4)$$

. Here, the accepted optical bolometric correction $L_{\text{bol}} \sim 10 \times L_{5100}$ is mainly from the statistical properties of spectral energy distributions of a sample of low redshift quasars discussed in Richards et al. (2006) and from the more recent discussed results in Netzer (2020) based on theoretical calculations. Moreover, Duras et al. (2020) have shown that the optical bolometric corrections appear to be fairly constant. Therefore, as commonly applied in the literature (Kaspi et al. 2000; Shen et al. 2011), we safely accepted the optical bolometric correction $L_{\text{bol}} \sim 10 \times L_{5100}$.

Based on the calculated M_{BH} and \dot{M}_{Edd} , the Spearman Rank correlation coefficients are about 0.15 ($P_{\text{null}} \sim 4 \times 10^{-4}$) and 0.36 ($P_{\text{null}} \sim 1.3 \times 10^{-17}$) for the correlation between M_{BH} and ΔV and for the correlation between \dot{M}_{Edd} and ΔV , respectively, shown in Fig. 6. It is clear that rather than central BH masses, accretion rates have more important effects on the strong linear correlation shown in Fig. 5: more powerful accretion rates lead to more stronger blue-shifted [O III] components. Meanwhile, besides the moderate dependence

of Eddington ratios on the strong correlation between ΔV and σ , Fig. 7 shows the correlation between ΔV and continuum luminosity at 5100Å. The correlation is stronger, with Spearman Rank correlation coefficient of about 0.48 for all the 535 quasars and of about 0.49 for the 160 high-quality quasars. Therefore, rather than BH masses, Eddington ratios and continuum luminosities have more important roles on properties of broad blue-shifted [O III] components in quasars.

Moreover, we have checked effects of extinctions traced by Balmer decrements (flux ratios of narrow H α to narrow H β). Fig. 8 shows the correlation between Balmer decrement and ΔV of the 151 low-redshift quasars with reliable broad blue-shifted [O III] components and with reliable narrow H α and narrow H β emission lines, and of the 10 low-redshift quasars with reliable broad red-shifted [O III] components and with reliable narrow H α and narrow H β emission lines. The Spearman Rank correlation coefficients are about 0.12 and -0.07 for the quasars with broad blue-shifted and with broad red-shifted [O III] components, respectively. The mean Balmer decrements are about 4.71 and 4.77 for the quasars with broad blue-shifted and with broad red-shifted [O III] components, respectively. Therefore, there are few effects of extinctions on the linear correlation between ΔV and σ . And moreover, in spite of less number of quasars with broad red-shifted [O III] components, there should be no different effects of extinctions on broad blue-shifted and broad red-shifted [O III] components. Here, the emission lines around H α are measured as what we have done to measure emission lines around H β . There are two (or more, if necessary) Gaussian components applied to describe broad H α , one narrow Gaussian component applied to describe narrow H α , two Gaussian components applied to describe [N II] $\lambda 6548, 6583\text{\AA}$ doublet, two Gaussian components applied to describe [S II] $\lambda 6716, 6732\text{\AA}$ doublet and one power law component applied to describe continuum emissions. As an example, Fig. 9 shows the best fitted results to the emission lines around H α in the quasar SDSS 1846-54173-0426.

Furthermore, as more recent discussed properties of [O III] emissions in Mullaney et al. (2013); Harrison et al. (2014); Kakkad et al. (2016); Wylezalek et al. (2020), the parameter w_{80} has been well applied to parameterise the velocity width of asymmetric [O III] emission lines, which refers to the velocity width that encloses 80% of the total [O III] flux. Here, two parameters of w_{80} and w_{20} of the [O III] emission lines are calculated in the SDSS quasars, where w_{20} refers to the velocity width that encloses 20% of the total [O III] flux. Then, rather than the line width of broad [O III] components applied, Fig. 10 shows the correlation between w_{80} (w_{20})

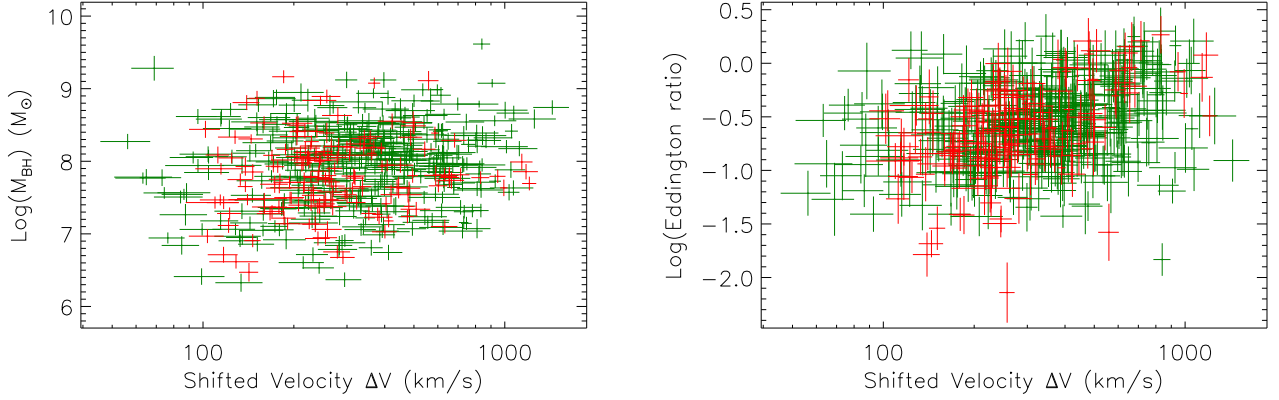


Figure 6. On the correlation between BH mass and ΔV (left panel) and between Eddington ratio and ΔV (right panel). In each panel, Dots plus error bars are for all the 535 quasars, red dots plus error bars are for the 160 high-quality quasars.

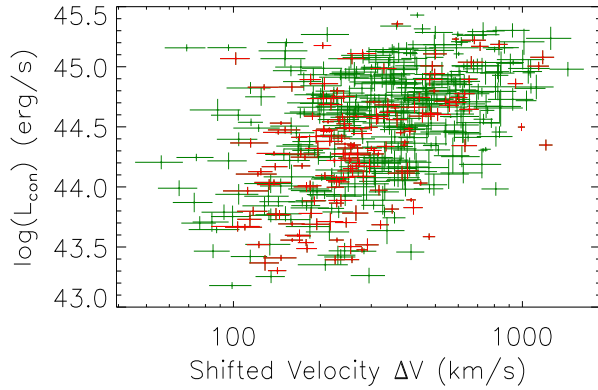


Figure 7. On the correlation between continuum luminosity and ΔV . Dots plus error bars are for all the 535 quasars, red dots plus error bars are for the 160 high-quality quasars.

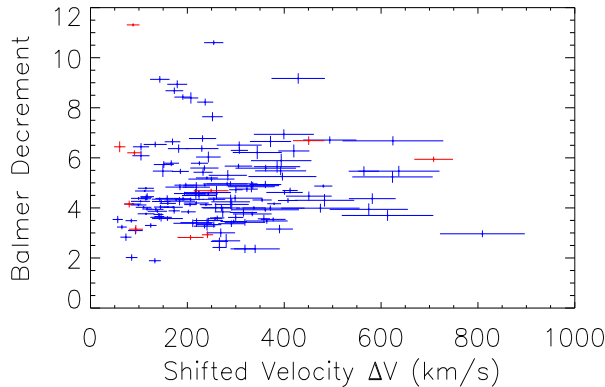


Figure 8. On the dependence of ΔV on Balmer decrements, symbols in blue and in red are for the quasars with broad blue-shifted [O III] components, and for the quasars with broad red-shifted [O III] components, respectively.

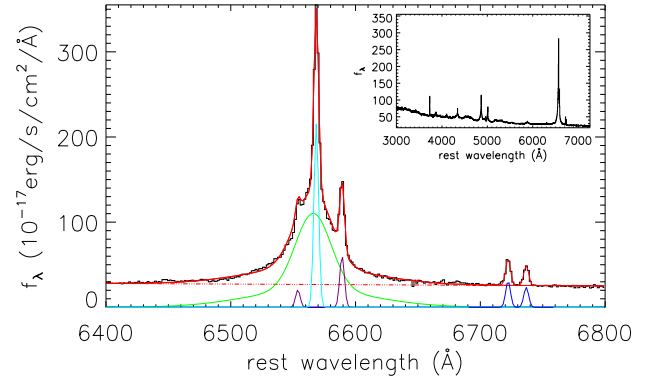


Figure 9. An example on the best fitted results to the emission lines around $H\alpha$ in the quasar SDSS 1846-54173-0426. In the figure, solid line in black and solid line in red show the line spectrum and the best fitted results, double-dot-dashed red line shows the determined power law continuum emissions, solid green line shows the determined broad $H\alpha$, solid purple lines and in blue show the determined [N II] and [S II] $\lambda 6717, 6731\text{\AA}$ doublets, solid cyan line shows the determined narrow $H\alpha$, respectively. In the top-right corner, the full spectrum with few contributions of stellar lights has been shown.

and ΔV , which can be well described by

$$\begin{aligned} \log\left(\frac{w80}{\text{km/s}}\right) &= (1.26 \pm 0.04) + (0.68 \pm 0.02) \times \log\left(\frac{\Delta V}{\text{km/s}}\right) \\ \log\left(\frac{w20}{\text{km/s}}\right) &= (1.22 \pm 0.03) + (0.41 \pm 0.02) \times \log\left(\frac{\Delta V}{\text{km/s}}\right) \end{aligned} \quad (5)$$

, through the LTS technique. It is apparent that there are also two linear correlations, but the Spearman Rank correlation coefficient is about 0.79 ($P_{\text{null}} < 10^{-20}$) for the correlation between $w80$ and ΔV , larger than the coefficient of 0.63 for the correlation between $w20$ and ΔV . The stronger correlation on the parameter of $w80$ indicates broad blue-shifted [O III] component rather than the core [O III] components have more

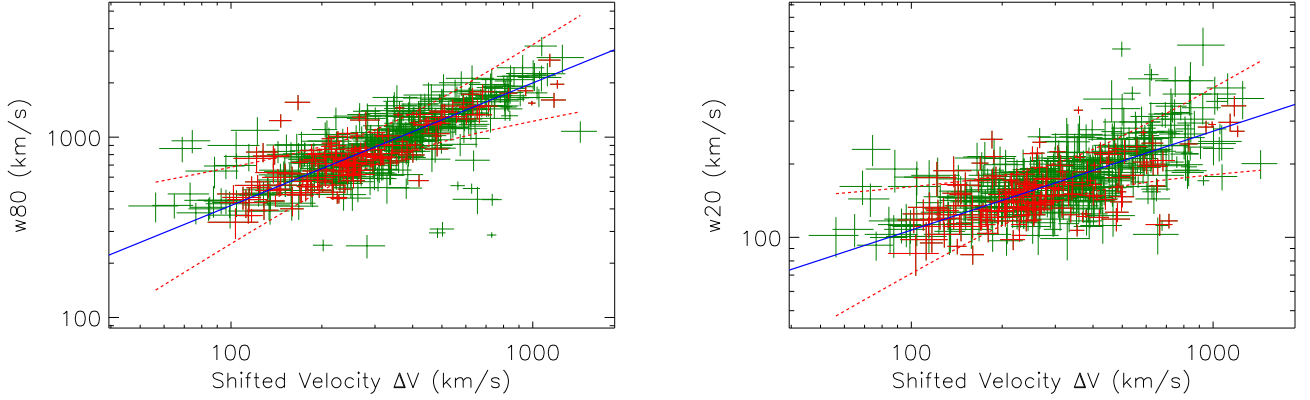


Figure 10. Left panel shows the correlation between $w80$ and ΔV . Right panel shows the correlation between $w20$ and ΔV . In each panel, solid blue line shows the best fitted results, dashed red lines show the corresponding 5σ confidence bands, respectively. In each panel, dots are for all the 535 quasars, red dots plus error bars are for the 160 high-quality quasars.

important contributions to the correlation between σ and ΔV shown in Fig. 5.

5. CONCLUSIONS

Finally, we give our main conclusions as follows. Based on a large sample of 535 SDSS quasar with reliable broad blue-shifted [O III] components, a strong linear correlation with Spearman Rank correlation coefficient 0.75 can be clearly confirmed between shifted velocity and line width of the broad blue-shifted [O III] components, which can be explained under the assumption of AGN-feedback driven outflows. Meanwhile, through similar criteria, there are only 20 SDSS quasars with reliable broad red-shifted [O III] components, and there is no positive correlation between shifted velocity and line width of the broad red-shifted [O III] components, providing strong evidence against the blue-shifted [O III] components related to local flows in NLRs. Therefore, strong broad blue-shifted [O III] components can be treated as better indicator of

outflows related to central engine in AGN. Moreover, stronger dependence of Eddington ratios and continuum luminosities can be found on the correlation between ΔV and σ of the broad blue-shifted [O III] components in quasars, indicating Eddington ratios and continuum luminosities have more important roles on properties of blue-shifted [O III] components in quasars.

ACKNOWLEDGEMENTS

Zhang gratefully acknowledges the anonymous referee for giving us constructive comments and suggestions greatly improving our paper. Zhang acknowledges the kind financial support from Nanjing Normal University and kind support from the Chinese grant NSFC-11973029. This paper has made use of the data from the SDSS projects. The SDSS-III web site is <http://www.sdss3.org/>. SDSS-III is managed by the Astrophysical Research Consortium for the Participating Institutions of the SDSS-III Collaboration.

REFERENCES

- Abazajian, K.; Adelman-McCarthy, J. K.; Agüeros, M. A.; et al., 2003, *AJ*, 126, 2081
- Alam, S., et al., 2015, *ApJS*, 219, 12
- Boroson, T., 2005, *AJ*, 130, 381
- Bruzual, G., & Charlot, S. 2003, *MNRAS*, 344, 1000
- Cappellari, M.; Scott, N.; Alatalo, K.; et al., 2013, *MNRAS*, 432, 1709
- Cid Fernandes, R., Mateus, A., Sodre, L., Stasinska, G., Gomes, J. M., 2005, *MNRAS*, 358, 363
- Cheung, E.; Bundy, K.; Cappellari, M.; et al., 2016, *Natur*, 533, 504
- Crenshaw, D. M.; Kraemer, S. B.; George, I. M., 2013, *ARA&A*, 41, 117
- Dimitrijevic, M. S.; Kovacevic, J.; Popovic, L. C.; Dacic, M.; Ilic, D., 2007, *MNRAS*, 374, 1181
- Duras, F.; Bongiorno, A.; Ricci, F.; et al., 2020, *A&A*, 636, 73
- Eun, D.; Woo, J.-H.; Bae, H.-J., 2017, *ApJ*, 842, 5
- Fabian, A. C., 2012, *ARA&A*, 50, 455
- Ferrarese, F. & Merritt, D., 2000, *ApJL*, 539, L9
- Foreman-Mackey, D.; Hogg, D. W.; Lang, D.; Goodman, J., 2016, *PASP*, 125, 306
- Ganguly, R.; Brotherton, M. S.; Cales, S.; et al., 2007, *ApJ*, 665, 990
- Gebhardt, K.; Bender, R.; Bower, G.; et al., 2000, *ApJL*, 539, L13
- Green, J. E., Ho, L. C., 2005, *ApJ*, 630, 122
- Gupta, Neeraj; Srianand, R.; Saikia, D. J., 2005, *MNRAS*, 361, 451

Table 1. Parameters of the 535 SDSS quasars with broad blue-shifted [O III] components

pmf	z	ΔV km/s	σ km/s	$\log(L_{\text{con}})$ erg/s	$\log(M_{\text{BH}})$ M_{\odot}	$\log(\dot{M}_{\text{Edd}})$	w80 km/s	w20 km/s
0274-51913-0388	0.256	392±51	478±28	44.07±0.06	7.75	0.111	870	158
0276-51909-0038	0.187	207±15	330±19	44.09±0.02	7.39	0.086	660	132
0282-51658-0138	0.268	512±50	669±75	44.30±0.04	8.01	0.094	1385	229
0285-51930-0280	0.259	238±17	364±22	44.58±0.03	8.40	0.087	515	133
0291-51928-0456	0.089	208±41	595±40	43.35±0.05	7.63	0.092	1035	117
0294-51986-0528	0.275	439±74	756±37	44.61±0.06	8.33	0.099	1491	263
0299-51671-0098	0.325	1117±165	958±98	44.83±0.10	8.17	0.104	2246	410
0299-51671-0251	0.385	389±36	573±83	44.94±0.03	8.20	0.098	1304	185
0301-51641-0151	0.163	223±42	421±25	43.93±0.05	7.42	0.097	908	141
0309-51994-0116	0.132	144±13	320±24	43.76±0.03	8.30	0.063	515	114

Notice: Col(1) shows the information of SDSS plate-mjd-fiberid, Col(2) shows the information of redshift, Col(3) shows the shifted velocity of the broad [O III] components relative to the core [O III] components, Col(4) shows the line width of the broad [O III] components, Col(5) shows the information of continuum luminosity, Col(6) shows the information of virial BH masses, Col(7) shows the information of Eddington ratios, Col(8) and Col(9) show the information of w80 and w20.

Here, parameters of only 10 of the 535 quasars are listed in the table. The full table can be downloaded from <https://pan.baidu.com/s/1gG85QpuXBDfa4NRb5dQHvg> with access code xip3.

Harrison, C. M.; Alexander, D. M.; Mullaney, J. R.; Swinbank, A. M., 2014, MNRAS, 441, 3306
Holt, J.; Tadhunter, C. N.; Morganti, R., 2008, MNRAS, 387, 639
Kaspi, S.; Smith, P. S.; Netzer, H.; et al., 2000, ApJ, 533, 631
Kauffmann, G., et al. 2003, MNRAS, 346, 1055
Kakkad, D.; Mainieri, V.; Padovani, P.; et al., 2016, A&A, 592, 148
King, A. R.; Zubovas, K.; Power, C., 2011, MNRAS Letter, 415, 6
King, A.; Pounds, K., 2015, ARA&A, 53, 115
Kormendy, J. & Ho, L. C., 2013, ARA&A, 51, 511
Kovacevic, J., Popovic, L. C., Dimitrijevic, M. S., 2010, ApJS, 189, 15
Martin-Navarro, I.; Brodie, J. P.; Romanowsky, A. J.; Ruiz-Lara, T.; van de Ven, Glenn, 2018, Natur, 553, 307
Mullaney, J. R.; Alexander, D. M.; Fine, S.; et al., 2013, MNRAS, 433, 622
Netzer, H., 2020, MNRAS, 488, 5185
Page, M. J.; Symeonidis, M.; Vieira, J. D.; et al., 2012, Natur, 485, 213
Perna, M.; Brusa, M.; Cresci, G.; et al., 2015, A&A, 574, 82
Peterson, B. M.; Ferrarese, L.; Gilbert, K. M., et al., 2004, ApJ, 613, 682
Rakshit, S.; Stalin, C. S.; Chand, H.; Zhang, X. G., 2017, ApJS, 229, 39
Shen, Y.; Richards, G. T.; Strauss, M. A.; et al., 2011, ApJS, 194, 45
Sergeev, S. G.; Pronik, V. I.; Malkov, Y. F.; Chuvaev, K. K., 1997, A&A, 320, 405

Richards, G. T., et al., 2002, AJ, 123, 2945
Richards, G. T.; Lacy, M.; Storrie-Lombardi, L. J.; et al., 2006, ApJS, 166, 470
Ross, N. P., et al., 2012, ApJS, 199, 3
Schmidt, E. O.; Oio, G. A.; Ferreira, D.; Vega, L.; Weidmann, W., 2018, A&A, 615, 13
Tadhunter, C.; Wills, K.; Morganti, R.; Oosterloo, T.; Dickson, R., 2001, MNRAS, 327, 227
Tombesi, F.; Meléndez, M.; Veilleux, S.; et al., 2015, Natur, 519, 436
Veilleux, S.; Cecil, G.; Bland-Hawthorn, J., 2005, ARA&A, 43, 769
Vestergaard, M., Peterson, B. M. 2006, ApJ, 641, 689
Wylezalek, D.; Flores, A. M.; Zakamska, N. L.; Greene, J. E.; Riffel, R. A., et al., 2020, MNRAS, 492, 4680
Woo, J.-H.; Bae, H.-J.; Son, D.; Karouzos, M., 2016, ApJ, 817, 108
Zakamska, N. L.; Hamann, F.; Paris, I.; et al., 2016, MNRAS, 459, 3144
Zhang, X. G., 2014, MNRAS, 438, 557
Zhang, X. G., Feng, L. L., 2016, MNRAS, 457, 3878
Zhang, X. G. & Feng, L. L., 2017, MNRAS, 468, 620
Zhang, X. G.; Bao, M.; Yuan, Q. R., 2019, MNRAS Letter, 490, 81